ISSN (Print) 1226-1750
ISSN (Online) 2233-6656
Journal of Magnetics 24(1), 184-189 (2019) https://doi.org/10.4283/JMAG.2019.24.1.184

Numerical Calculation of Stator End Leakage Reactance of Permanent Magnet Machines with Concentric Winding

Xiaoqin Zheng, Wen Zhang, Xinzhen Wu*, and Ronggang Ni

College of Electrical Engineering, Qingdao University, Qingdao 266071, China

(Received 11 July 2018, Received in final form 19 December 2018, Accepted 20 December 2018)

Concentric winding has been widely used in small capacity AC motors due to its excellent performance. In this paper, a numerical calculation method based on the magnetic vector potential is proposed to calculate the stator end leakage reactance of concentric winding. In this case, the basic unit of numerical calculation becomes the coil group rather than the coil since concentric windings have different coil sizes. The calculated stator end leakage reactance of a prototype three-phase permanent magnet machine with concentric winding is validated using the finite element method. Compared to 3D electromagnetic field calculation, the proposed method does not require a complex modeling process and is therefore highly efficient computationally, requiring only a fraction of the calculation time.

Keywords : concentric winding, magnetic vector potential, coil group, finite element method

1. Introduction

The stator winding plays an important role in the electrical and mechanical energy conversion. In order to deal with issues such as harmonic weakening, cooling, insulation and others, various winding configurations may be adopted [1-3]. Compared to other forms of winding, concentric winding not only limits higher harmonics but also requires less wiring material. Therefore, the concentric winding has been widely used in small capacity AC motors due to the excellent performance it offers [4, 5].

No matter which winding configuration employed, the calculation of the stator leakage reactance is the basis of motor design. The accuracy of the parameter calculation is very important for the performance analysis of steady and transient operation of motors [6-10]. Generally, the stator leakage reactance is composed of stator slot leakage reactance, harmonic leakage reactance and end-winding leakage reactance [11-13]. Many scholars have put considerable effort in parameter calculation methods and some very effective methods have been obtained. The calculation methods of slot leakage reactance and harmonic leakage reactance are quite mature, however, the calculation of end-winding leakage reactance is still under discussion [14-17]. Most of researches focus on the calculation of end-winding leakage reactance for normative lap winding while calculation methods of concentric winding are scarce, due to the fact that concentric winding has a special winding arrangement and different coil sizes [18, 19]. Although some empirical equations have been obtained according to the simplified concentric winding theory and many experiments, the complexity of the end-winding connection cannot be fully expressed by empirical equations. Moreover, the three-dimensional electromagnetic field can also be used to calculate the stator end leakage reactance, but the model is too complex and involves a high computational load [20, 21]. Therefore, it is difficult to satisfy the requirement of machine design using electromagnetic field calculation.

In this paper, a numerical calculation method based on the magnetic vector potential is proposed to calculate the stator end leakage reactance of concentric winding. The proposed method is fit for different forms of concentric winding and thus is more widely applicable, flexible and efficient. Taking a three-phase permanent magnet machine with concentric winding as an example, the calculation result is validated using a three-dimensional electromagnetic field by finite element method.

*Corresponding author: Tel: +86-85953672
Fax: +86-85953672, e-mail: wuxinzhen81@163.com

This paper was presented at the IcAUMS2018, Jeju, Korea, June 3-7, 2018.

2. Concentric Wingding Configuration

The prototype permanent magnet machine adopts single-layer concentric winding. The design parameters of the concentric winding are listed in Table 1. In order to show the winding connection more clearly, the two-pole coil distribution for phases *A*, *B*, and *C* are shown in Fig. 1, where the positive current directions in the coil and each phase winding are also shown.

As shown in Fig. 1, each phase winding consists of three coils with different sizes. Take phase *A* as an example. The smallest pitch of coil sides located in No. 3 and 10 slots is 7. The larger one of coil sides located in No. 2 and 11 slots is 9. The largest pitch of coil sides located in No. 1 and 12 slots is 11. According to the difference of the pitches, the concentric coils can be classified into different types. Thus there are three coil types for the concentric winding of phases *A*, *B*, and *C* in Fig. 1. The pitches equal to 7, 9, and 11 are named type I, type II, and type III coil, respectively and have the same symmetrical axis. Thus, these coil types can be concatenated into a coil group. Although different type coils may be used for each phase concentric winding, the structure of the coil groups is the same. Therefore, in this paper, the basic unit used for the numerical calculations of concentric winding is the coil group rather than the coil.

Table 1. Parameters of the prototype concentric winding.

	Value
Number of stator slots	36
Number of poles	4
Pole pitch	9
Number of slots per pole per phase	3
Number of conductors per slot	3
Number of parallel-circuits per phase	1

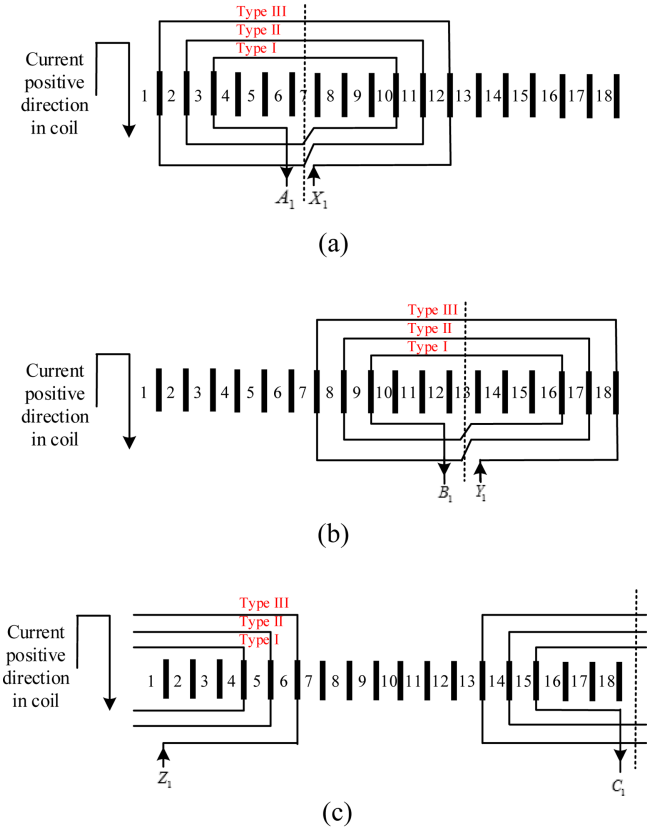

Fig. 1. (Color online) Two-pole concentric winding coil distribution.

3. Calculation of Stator End Leakage Reactance

3.1. Division of End-Winding

The pairwise mutual inductance between coil groups must be calculated. Fig. 2 shows the 3-D coordinate system for the end-winding. For simplicity, only the type III coil of coil group 1 and type I coil of the coil group 2 are drawn. The axis of the machine's end surface is regarded as the coordinate origin, the outward direction of the machine shaft is regarded as x-axis positive direction, the direction from origin to the center line of the two coil sides is regarded as the z-axis positive direction, and the YZ plane overlaps the machine end surface, respectively.

First, the end of all the three types coils in coil group 1 should be divided respectively. We consider the type III coil in coil group 1 as an example, since the divisions of different types coils are the same. To consider the influence of the machine-end magnetic field from air-gap to stator and rotor iron core, the air-gap currents and their image currents are introduced. The original currents in the end-winding are highlighted in red line segments *AB*, *BC* and *CD*. The image currents of original current are shown

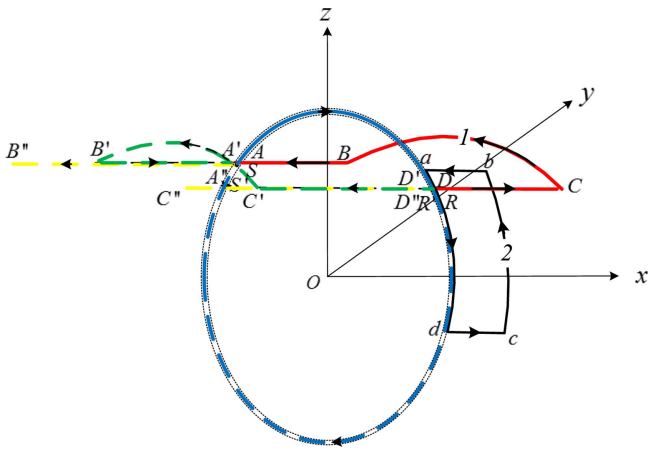

Fig. 2. (Color online) End-winding with coordinate systems.

by the green line segments *A'B'*, *B'C'* and *C'D'*. The air-gap currents and their image currents are highlighted in the internal *SR* and *S'R'* and external *RS* and *R'S'* blue line segments. The image currents in slots are shown using the yellow line segments *A"B"* and *C"D"*. The number of the whole line segments of the type III coil are 12 and thus the total number of segments of coil group 1 is 36 obtained by summing all three coil types. Each line segment k (k = 1, 2,…, 36) can be further divided into M_k sections. Therefore, the first and end point three-dimensional coordinates (x_{1km}, y_{1km}, z_{1km}) and ($x_{1k(m+1)}$, $y_{1k(m+1)}$, $z_{1k(m+1)}$) of line segment k section m in coil group 1 are known. The corresponding vector is

$$\begin{aligned}\boldsymbol{l}_{1km} &= (x_{1k(m+1)} - x_{1km})\boldsymbol{x} + (y_{1k(m+1)} - y_{1km})\boldsymbol{y} \\ &\quad + (z_{1k(m+1)} - z_{1km})\boldsymbol{z}\end{aligned} \tag{1}$$

where $\boldsymbol{x}$, $\boldsymbol{y}$, and $\boldsymbol{z}$ are the unit vectors in the x, y, and z directions, respectively.

Then, coil group 2 is selected as the closed integral path, and we consider the type I as an example. The integral path of the type I coil is shown by the black line segments *ab*, *bc*, *cd*, and *da*. The number of the line segments of the type I coil are 4 and thus the total number of segments in coil group 2 is 12, if we take into account all three types coils. Each line segment g (g = 1, …, 12) can be sequentially divided into N_g subsections. Similarly, the first and end point three-dimensional coordinates (x_{2gn}, y_{2gn}, z_{2kn}) and ($x_{2g(n+1)}$, $y_{2g(n+1)}$, $z_{2g(n+1)}$) of line segment g section n in coil group 2 are known, and the corresponding vector can be written as

$$\begin{aligned}\boldsymbol{l}_{2gn} &= (x_{2g(n+1)} - x_{2gn})\boldsymbol{x} + (y_{2g(n+1)} - y_{2gn})\boldsymbol{y} \\ &\quad + (z_{2g(n+1)} - z_{2gn})\boldsymbol{z}\end{aligned} \tag{2}$$

Third, the magnetic vector potential should be calculated. The distance r_{2gn1km} between the middle points of line segment k section m in coil group 1 and line segment g section n in coil group 2 can be determined after the corresponding vectors are known, and is distance between the two vectors. It is worth noting that the integral path in coil group 2 should be selected along the inner side of the coil to avoid the value of r_{2gn1km} becoming to zero. Thus the minimum value of r_{2gn1km} is the radius of the coil.

Therefore, the magnetic vector potential in middle point of segment g section n in coil group 2 produced by the current in line segment k section m in coil group 1 is

$$\boldsymbol{A}_{2gn1km} = \frac{\mu_0}{4\pi}\frac{I_{1k}\boldsymbol{l}_{1km}}{r_{2gn1km}} \tag{3}$$

The value of current I_{1k} in (3) is different for each line segment k. Assuming the current in each turn coil is I_1 and the number of turns is W_{III}, the current in the whole section in a type III coil is

$$I_{1k} = \begin{cases} W_{\mathrm{III}}I_1 & k = 1, 2, 3 \\ W_{\mathrm{III}}I_1 & k = 4, 5, 6 \\ \dfrac{(Z_1 - y_{\mathrm{III}})W_{\mathrm{III}}I_1}{Z_1} & k = 7, 9 \\ \dfrac{y_{\mathrm{III}}W_{\mathrm{III}}I_1}{Z_1} & k = 8, 10 \\ 2W_{\mathrm{III}}I_1 & k = 11, 12 \end{cases} \tag{4}$$

where Z_1 is the number of stator slots, y_{III} is the pitch of the type III coil, y_{III} should be changed to y_{I} and y_{II} for the type I and type II coil, while W_{III} should be replaced with W_{I} and W_{II} for the type I and type II coils, respectively.

3.2. End Leakage Inductance between Two Coil Groups

As mentioned above in section II and shown in Fig. 1, there are three same coil groups under a pair of poles. Thus there are six same coil groups in all for prototype concentric winding with four poles listed in Table 1. Consequently, there are 36 end leakage inductances m_{ji} between coil group i (i = 1, 2,…, 6) and coil group j (j = 1, 2,…, 6), many of which have the same value. For example, $m_{11} = m_{22} = m_{33} = m_{44} = m_{55} = m_{66}$, $m_{12} = m_{21} = m_{23} = m_{32} = m_{34} = m_{43} = m_{45} = m_{54} = m_{56} = m_{65} = m_{61} = m_{16}$, etc. Actually, only m_{11}, m_{12}, m_{13}, and m_{14} need to be calculated here. We consider the calculation process of m_{21} for instance.

The magnetic vector potential in the middle point of line segment g section n in coil group 2 produced by the currents in all sections in coil group 1 is

$$\boldsymbol{A}_{2gn1} = \sum_{k=1}^{36}\sum_{m=1}^{N_k}\boldsymbol{A}_{2gn1km} \tag{5}$$

Based on magnetic vector theory, the circulation of magnetic vector potential along any closed path is equal to magnetic flux through any surface bounded by this path. Thus, the magnetic linkage of coil group 2 produced by currents in coil group 1 is

$$\psi_{21} = \sum_{g=1}^{12}\left[W_{2g}\sum_{n=1}^{N_g}(\boldsymbol{A}_{2gn1}\cdot\boldsymbol{l}_{2gn})\right] \tag{6}$$

where W_{2g} is equal to W_{I}, W_{II} and W_{III} when the value of g is 1-4, 5-8, and 9-12 respectively.

The end leakage inductance m_{21} between coil group 1 and coil group 2 is

$$m_{21} = \frac{1}{I_1}\frac{\mu_0}{4\pi}\sum_{g=1}^{12}\left[W_{2g}\sum_{n=1}^{N_g}\left(\left(\sum_{k=1}^{36}\sum_{m=1}^{N_k}\frac{I_{1k}\boldsymbol{l}_{1km}}{r_{2gn1km}}\right)\cdot\boldsymbol{l}_{2gn}\right)\right] \tag{7}$$

The actual end leakage inductance between two coil groups is twice the value of (7), as each coil group has two ends.

3.3. Each Phase End Leakage Reactance

To calculate the end leakage reactance between two phases for concentric winding, an incidence matrix **B** associating the phase winding with each coil group is introduced.

According to the incidence matrix of the loop and branch circuit in the circuit network theory, each coil group is regarded as a branch circuit and each phase winding as a loop circuit. The elements in **B** are 1, −1 or 0 corresponding to currents in the same or opposite directions or those without any association between each loop and branch circuit, respectively. For a single layer concentric winding 3-phase permanent magnet machine with two pairs of poles, the incidence matrix **B** is of order 3×6.

According to the positive directions of currents shown in Fig. 1, the incidence matrix **B** is

$$\mathbf{B}=\begin{bmatrix}1&0&0&1&0&0\\0&1&0&0&1&0\\0&0&1&0&0&1\end{bmatrix} \tag{8}$$

We need to point out that elements equal to −1 do not exist in **B** for this single layer concentric winding, however elements equal to 1, −1 or 0 exist in double layer concentric winding configurations.

Assuming the number of parallel-circuits per phase is a, the end leakage inductance between two phases for concentric winding is

$$M_{\mu\nu}=\frac{1}{a^2}\sum_{i=1}^{6}\sum_{j=1}^{6}b_{\mu i}b_{\nu j}m_{ji} \tag{9}$$

where $b_{\mu i}$ and $b_{\nu j}$ are respectively the elements of row m column i and row n column j in **B**, where m and n are equal to 1, 2, and 3 and correspond to phase A, B, and C respectively. Similarly, M_{23} is the mutual inductance between phase B and C.

The 3×3 order end leakage inductance matrix can be calculated from (9). Therefore, each phase end leakage reactance by summing the effect of all the three phase (converted to phase A) is

$$X_{se}=2\pi f_1\sum_{\nu=1}^{3}M_{1\nu}\cos\left[(\nu-1)\frac{2\pi}{3}\right] \tag{10}$$

Depending on the actual size of the end-winding, the section number of original currents and integral path of straight line segments along x-axis are set to n, the section number of arc line segments are $4n$, the section number of internal air-gap current and its image current are $4n$, and the section number of external air-gap current and its image current are $12n$. The relationship between the section number n and the calculated phase end leakage reactance X_{se} is shown in Fig. 3.

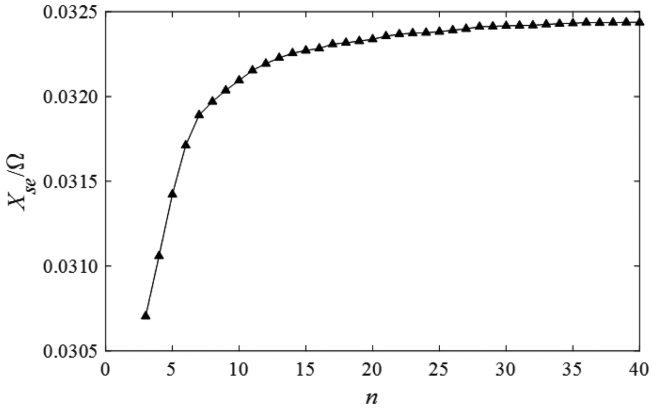

Fig. 3. Relationship between end-winding leakage reactance and section number.

As shown in Fig. 3, the calculated results tend to be stable with the increase of the section number. When the section number is larger than 30, the result tends to stabilize. The end leakage reactance of the prototype permanent magnet machine with concentric winding is 0.0324 Ω when the section number n is 40.

4. Finite Element Method Validation

To verify the above analysis, the 3-D electromagnetic field calculation by finite element method (FEM) is adopted. Fig. 4 shows the stator end-winding FEM model.

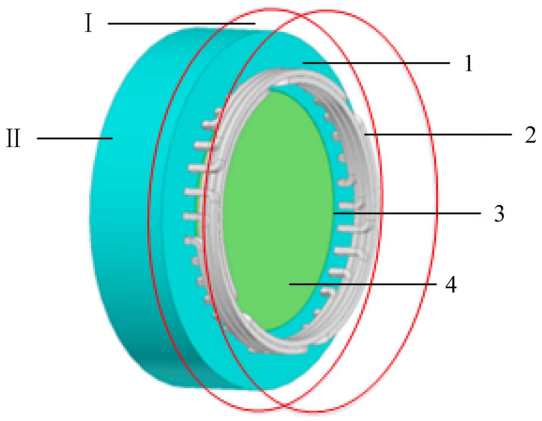

1-Stator iron core; 2-Concentric winding; 3-air-gap;4-Rotor iron core; I-Calculation region of end-winding; II- Calculation region of end stator and rotor iron core.

Fig. 4. (Color online) Stator end-winding FEM model and calculation region.

Here, we assume that the three-phase currents in the concentric winding are

$$\begin{cases} i_A = I_m \cos(\omega t) \\ i_B = I_m \cos(\omega t - 120^\circ) \\ i_C = I_m \cos(\omega t - 240^\circ) \end{cases} \tag{11}$$

where I_m is the amplitude of rated current.

For the symmetrical three-phase concentric winding, the relationships between end self-leakage inductance and end mutual leakage inductance are

$$\begin{cases} L_{AA} = L_{BB} = L_{CC} = L \\ M_{AB} = M_{AC} = M_{BC} = M \end{cases} \tag{12}$$

where L_{AA}, L_{BB} and L_{CC} are the end self-leakage inductances, and M_{AB}, M_{BC} and M_{AC} are the end mutual leakage inductances.

Thus the total energy of the end magnetic field is

$$\begin{aligned} W &= \frac{1}{2}(L_{AA}i_A^2 + L_{BB}i_B^2 + L_{CC}i_C^2) + M_{AB}i_Ai_B + M_{BC}i_Bi_C + M_{CA}i_Ci_A \\ &= \frac{3}{4}(L-M)I_m^2 \\ &= \frac{3}{4}L_{se}I_m^2 \end{aligned} \tag{13}$$

where L_{se} is the end leakage inductance of the concentric winding.

Then, the stator end leakage reactance can be indirectly calculated using the end-winding magnetic field energy.

$$X_{se} = \omega L_{se} = \frac{4\omega W}{3I_m^2} \tag{14}$$

The calculation result of the end-winding magnetic field distribution and energy density are shown in Fig. 5 and Fig. 6 respectively.

Judging from the results in Fig. 5 and Fig. 6, the magnetic field energy is mainly distributed in the end-winding and air-gap. The stator end leakage reactance can be obtained by substituting the calculated magnetic field energy into (14). Table 2 shows the results between the proposed method and FEM.

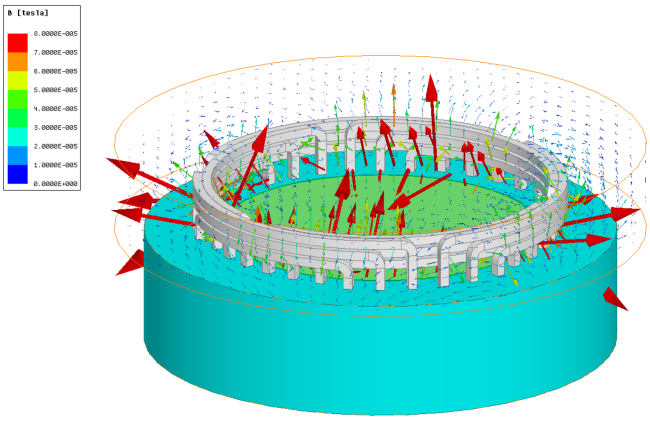

Fig. 5. (Color online) Calculation result of the end magnetic field distribution.

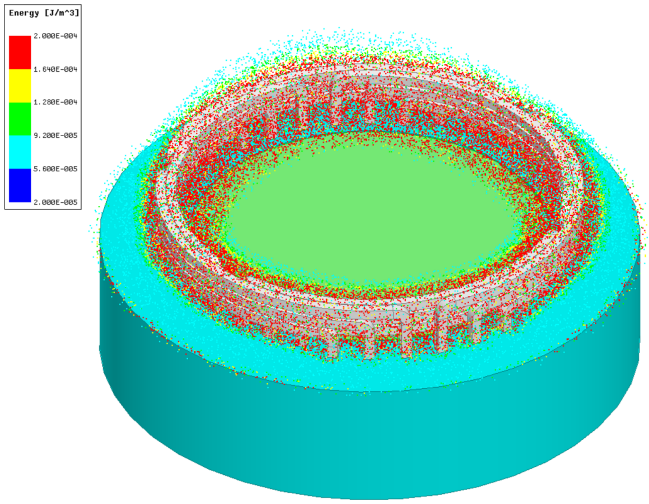

Fig. 6. (Color online) Calculation result of the end magnetic field energy density.

Table 2. Result Comparisons between Two Different Methods.

	Proposed method	FEM	Error
Stator end leakage reactance	0.0324Ω	0.0345Ω	–6.09%

As shown in Table 2, the FEM calculated result of a permanent magnet machine with single-layer concentric winding verifies the validity of the proposed method. It is well known that 3-D electromagnetic field calculation is time-consuming. The FEM calculation time for the case presented in this paper took more than 5 hours using a Dell Tower 7910 work station. However, the proposed methods' computational time only takes a few minutes. Therefore, the numerical calculation method proposed in this paper is feasible and practical with high calculation accuracy and efficiency.

5. Conclusion

A numerical calculation method based on the magnetic vector potential is proposed to calculate the stator end leakage reactance of concentric windings. In this method, the coil group becomes the basic calculation unit since the concentric windings have different coil sizes. In addition, an incidence matrix **B** is introduced to calculate the end leakage reactance between two phases.

The proposed method is not only suitable for concentric

windings but also for lap windings. The basic calculation unit for lap winding is still the coil, as lap windings have the same coils. In this case, the corresponding incidence matrix **B** is associated the phase winding with each coil, but the calculation process for the lap winding is simpler.

Finally, through a comparison between the proposed numerical calculation and a 3-D electromagnetic field calculation, the proposed numerical calculation not only have high accuracy but also is very efficient computationally. Consequently, the proposed method is suitable for machine design.

Acknowledgments

This work was supported by the National Natural Science Foundation of China under Grant 51677092 and China Postdoctoral Science Foundation Grant 2018M642610.

References

[1] F. Barrero and M. J. Duran, IEEE Trans. Ind. Electron. **63**, 1 (2016).
[2] M. J. Duran and F. Barrero, IEEE Trans. Ind. Electron. **63**, 1 (2016).
[3] X. Longya and Y. Lurong, IEEE Trans. Ind. Appl. **31**, 1 (1995).
[4] J. Pyrhönen, T. Jokinen, T. Jokinen, and V. Hraboveová, Chichester: Jone Wiley & Sons (2008).
[5] I. Boldea and S. A. Nasar, Second Edition. Boca Raton: CRC Press (2010).
[6] L. Nicolas, B. Thierry, N. M. Babak, T. Noureddine, M. T. Farid, and C. Guy, IEEE Trans. Magn. **48**, 2 (2012).
[7] L. Chunyan, F. Guodong, M. Kaushik, and C. K. Narayan, IEEE Trans. Energy Conversion **32**, 3 (2017).
[8] M. Anees and D. Sinisa, IEEE Transactions on Energy Conversion (2018).
[9] J. Shaofeng, Q. Ronghai, and L, Jian, IEEE Energy Conversion Congress and Exposition (2015).
[10] B. Feifei, H. Yuwen, H. Wenxin, and Z. Shenglun, IEEE Trans. Ind. Electron. **61**, 8 (2014).
[11] B. T. Araujo, M. S. Han, B. Kawkabani, and E. C. Bortoni, International Conference on Electrical Machines (2016).
[12] A. L. Thomas, Introduction to AC Machine Design (2018).
[13] L. Yanping, G. Lianlian, L. Cangxue, and H. Yonglu, IEEE Trans. Ind. Electron. **65**, 2 (2018).
[14] L. Yanping, B. Xu, Y. Honghao, W. Lei, and Y. Lichao, IEEE Trans. Ind. Electron. **61**, 10 (2014).
[15] W. Xinzhen and W. Xiangheng, Proceedings of the CSEE **27**, 12 (2007).
[16] W. Xinzhen and W. Xiangheng, Proceedings of the CSEE **27**, 21 (2007).
[17] W. Xinzhen and W. Xiangheng, Proceedings of the CSEE **27**, 24 (2007).
[18] X. Yongming, M. Dawei, and W. Jiabin, International Conference on Energy and Environment Technology 2 (2009).
[19] C. Tom, E. Fred, and P. Jeff, IEEE Trans. Magn. **44**, 11 (2008).
[20] W. Shanming, W. Xiangheng, L. Yixiang, S. Pengsheng, M. Weiming, and Z. Gaifan, Transactions of China Electrotechnical Society **16**, 2 (2001).
[21] G. Yuting, Q. Ronghai, and L. Dawei, Chinese Journal of Electrical Engineering **2**, 1 (2001).